Accepted Manuscript

Preparation and characterization of rod-like chitosan–quinoline nanoparticles as pH-responsive nanocarriers for quercetin delivery

Shahnaz Rahimi, Sepideh Khoee, Mehdi Ghandi

PII: S0141-8130(18)35290-5
DOI: https://doi.org/10.1016/j.ijbiomac.2019.01.137
Reference: BIOMAC 11570

To appear in: *International Journal of Biological Macromolecules*

Received date: 4 October 2018
Revised date: 10 January 2019
Accepted date: 24 January 2019

Please cite this article as: S. Rahimi, S. Khoee and M. Ghandi, Preparation and characterization of rod-like chitosan–quinoline nanoparticles as pH-responsive nanocarriers for quercetin delivery, International Journal of Biological Macromolecules, https://doi.org/10.1016/j.ijbiomac.2019.01.137

Preparation and characterization of rod-like chitosan–quinoline nanoparticles as pH-responsive nanocarriers for quercetin delivery

Shahnaz Rahimi,

School of Chemistry, College of Science, University of Tehran, Tehran, Iran

sh.rh1989@gmail.com

Sepideh Khoee*,

School of Chemistry, College of Science, University of Tehran, , PO Box 14155 6455, Tehran, Iran, Tel: (098) 21 61113301, Fax

Khoee@khayam.ut.ac.ir

Mehdi Ghandi,

School of Chemistry, College of Science, University of Tehran, Tehran, Iran

ghandi@khayam.ut.ac.ir

* Corresponding author

Abstract

Novel chitosan–quinoline nanoparticles as anticancer drug nanocarriers were prepared using 2-chloro-3-formylquinoline and 3-formylquinolin-2(1*H*)-one as non-toxic modifying agents via oil–in–water nanoemulsion technique. Chitosan–quinoline nanoparticles were characterized by FT–IR, UV–vis spectrophotometry, XRD, SEM, AFM and DLS techniques. The morphological and particle size studies demonstrated that drug–loaded chitosan–quinoline nanoparticles have a regular nanorod shape and monolithic structure with the desired particle size of 141 to 174.8 nm and a negative zeta potential of −2.4 to −14.1 mV. Drug loading capacity (LC) and encapsulation efficiency (EE) were achieved using quercetin as a hydrophobic anticancer drug and were about 4.8–9.6% and 65.8–77%, respectively. The *in vitro* release studies displayed great pH-sensitive release behavior. Evaluation of the anticancer efficacy of quercetin loaded chitosan–quinoline nanoparticles using the in vitro cytotoxicity studies against HeLa cells indicated that the chitosan nanoparticles are a promising candidate for the anticancer drugs delivery.

Keywords: Chitosan; 2-chloro-3-formylquinoline; 3-formylquinolin-2(1*H*)-one; nanorod shape; drug delivery system.

1. Introduction

Chitosan is a natural biopolymer generally produced by deacetylation of chitin with excellent accessibility, biodegradability, biocompatibility, nontoxicity and antimicrobial activity [1]. Chitosan has been extensively used as a material in numerous biomedical and pharmaceutical fields, such as gene delivery, biosensors, tissue engineering and drug delivery systems. Chitosan and its derivatives have received the most attention among researchers owing to its various physicochemical features and biological activities [2-6]. Due to its excellent adhesion property, chitosan can enhance the cell membrane permeability [7]. Accordingly, various drug carriers are designed using chitosan and its derivatives. Fu et al. developed chitosan hollow microspheres (CHM) as a new carrier for tough hydrophobic drugs based on an interfacial Schiff-base bonding reaction [8]. Liu et al. designed monodisperse core-shell chitosan microcapsules via a crosslinking reaction of O/W/O double emulsion of chitosan and terephthalaldehyde, which exhibited a pH-responsive burst release of hydrophobic drugs [9]. These findings show that chitosan and its derivatives are suitable candidates for drug carriers. However, concerns about the safety of chitosan particles remains owing to the toxicity of organic crosslinking agents especially glutaraldehyde, which causes adverse effects on the human body [10,11]. Natural and non-toxic products possessing biological properties can be used as crosslinking agents to overcome the potential side effects. Therefore, the choice of the appropriate crosslinking agent is a novel and interesting challenge for the preparation of chitosan nanoparticles [12,13].

Quinolines are important biological compounds because of their occurrence in a large number of natural products especially in alkaloids, and their broad range of applications in pharmaceuticals, medicine and agrochemicals [14,15]. Due to their good efficacy and desirable safety profiles, compounds containing quinoline have attracted considerable attention for their diverse bioactivities like antifungal [16], anti-inflammatory [17,18],

antimalarial [19], antiviral [20], antimicrobial [21,22], anticancer [23,24] and analgesic activities [18]. Moreover, quinoline and its derivatives have been widely utilized in medicinal chemistry due to the occurrence of their structure in the number of commercial drugs such as mefloquine [25], quinine [26], amodiaquine [27] and chloroquine [28]. Among the quinoline derivatives, 2,3-disubstituted quinolines and 3-substituted quinolin-2-ones have played an important role in the design and development of novel compounds with marvelous anticancer activities [29,30]. Inspired by the known properties of quinoline and its derivatives, we undertook a study for the synthesis of novel drug–loaded chitosan–quinoline nanoparticles with 2-chloro-3-formylquinoline (CFQ) and 3-formylquinolin-2(1*H*)-one (FQO) as non-toxic modifying agents via oil–in–water (O/W) nanoemulsion method. The obtained chitosan–quinoline nanoparticles were characterized by means of FT–IR, XRD, UV–vis, SEM imaging techniques and other spectroscopic methods. Quercetin was loaded into the modified chitosan nanoparticles as a model anticancer drug. Furthermore, the release of quercetin from the chitosan–quinoline nanoparticles was evaluated and cytotoxicity against HeLa cells was also investigated using MTT assay.

2. Experimental

2.1 Materials

Chitosan (CS) with low molecular weight (MW = 50,000–190,000 Da, degree of deacetylation: 85%), Dulbecco's Modified Eagle's medium (DMEM) and 3-(4,5-dimethylazolyl-2)-2,5-diphenyl tetrazolium bromide (MTT) were purchased from Sigma-Aldrich. Quercetin was purchased from Fluka Chemical Co. Phosphoryl chloride ($POCl_3$), N,N-dimethylformamide (DMF), acetanilide, glacial acetic acid (CH_3COOH, 100%), Tween 60 (polyoxyethylene sorbitan monostearate, HLB = 14.9), dichloromethane (CH_2Cl_2, 99%), ethanol (EtOH, 99%) and other commercially available chemicals were supplied from Merck Chemical Company and used without further purification.

2.2 Measurements

The ^{1}H NMR of the organic products was recorded on a Bruker 500 MHz NMR spectrometer using $CDCl_3$ as the solvent at 25 °C. Melting points were carried out by an Electrothermal model 9100 apparatus and are uncorrected. Mass spectra of the organic compounds were obtained using an HP (Agilent technologies) 5937 Mass Selective Detector. Fourier transform infrared (FT–IR) spectra were performed in KBr pellets by FT–IR spectrophotometer (IR Affinity, Shimadzu, Japan) using KBr in the range of 600–4000 cm^{-1}. The average particle size and zeta potential of the chitosan–quinoline nanoparticles were determined by dynamic light scattering (DLS, Brookhaven instrument, USA) at 25 °C in triplicate. Each sample was diluted to the desired concentration using deionized water and the analysis was carried out at a fixed scattering angle of 90°. Ultraviolet–visible (UV–vis) absorption spectra were determined on a UV-VIS spectrophotometer (Jasco V750, Jasco, Tokyo, Japan). The shape of the obtained nanoparticles was analyzed by scanning electron microscopy (FE–SEM) (HITACHI S–4160, Japan). Samples were mounted on an aluminium stub using a double adhesive carbon tape and then sputter–coated with gold before observations. X–ray diffraction (XRD) analysis of the samples was conducted by an X–ray diffractometer (Rigaku, Japan) with CuKα radiation as target. The measurement was carried out at a voltage of 40 kV and 40 mA current and 2θ angle range from 5° to 50° at a scanning speed of 4° min^{-1} at room temperature. The topography of the drug–loaded chitosan–quinoline nanoparticles was characterized by atomic force microscopy (AFM, ENTEGRA AFMNT–MDT, China) on a freshly cleaved mica substrate.

2.3 Synthesis and characterization of 2-chloro-3-formylquinoline

Dry DMF (2.7 mL, 34.65 mmol) was cooled to 0–5 ºC in a round bottom flask, and $POCl_3$ (9 mL, 98.28 mmol) was added dropwise by a dropping funnel to DMF with stirring. After stirring the solution for about 15 min, acetanilide (1.4 g, 10.37 mmol) was added and

the mixture heated at 75–80 °C for 8 h. The reaction mixture was then poured into crushed ice under vigorous stirring for about 30 minutes. The precipitate thus appeared was filtered, washed well with cold water and dried. Recrystallization of the crude compound from ethyl acetate finally afforded the product **1** in high yield (90 %), mp: 147–148 °C; FT–IR (KBr), ν, cm^{-1}: 1682 (HC=O), 943 (C–Cl); ^{1}H NMR (500MHz, $CDCl_3$): δ 7.61 (t, *J* = 7.3 Hz, 1H), 7.86 (t, *J* = 7.3 Hz, 1H), 7.95 (d, *J* = 8.1 Hz, 1H), 8.04 (d, *J* = 8.1 Hz, 1H), 8.72 (s, 1H), 10.52 (s, 1H); ESI-MS *m/z*: $[M+H]^+$calcd. for $C_{10}H_6ClNO$ = 191.01; found 191.3 (**Figure S1**).

2.4 Synthesis and characterization of 3-formylquinolin-2(1*H*)-one

A suspension of 2-chloro-3-formylquinoline (1 mmol) in acetic acid (70%, 10 mL) was stirred under reflux for 4–6 h. After completion as indicated by TLC, the reaction mixture was cooled to room temperature and the precipitated product filtered, washed with water and dried. (yield 93%; mp: 302–303 °C); FT–IR (KBr), ν, cm^{-1}: 3153 (N–H), 1666 (HC=O), 1623 NHC=O); ^{1}H NMR (500MHz, $CDCl_3$): δ 7.72 (t, *J* = 7.1 Hz, 1H), 7.93 (t, *J* = 7.1 Hz, 1H), 8.05 (d, *J* = 8.3 Hz, 1H), 8.14 (d, *J* = 8.3 Hz, 1H), 8.76 (s, 1H), 10.27–10.48 (br s, 1H), 10.63 (s, 1H); ESI-MS *m/z*: $[M+H]^+$calcd. for $C_{10}H_7NO_2$ = 173.1; found 173.0 (**Figure S2**).

2.5 Preparation of chitosan-quinoline nanoparticles

Chitosan–quinoline nanoparticles were prepared via the O/W nanoemulsion system. Briefly, chitosan (1%, w/v) was dissolved in dilute acetic acid solution (0.7%, v/v) at ambient temperature and vigorously stirred overnight (1400 rpm). After addition of Tween 60 (1%, w/v), the mixture was sonicated in an ultrasonic probe for 15 min until the aqueous phase mixture became homogeneous. Quercetin was dissolved in EtOH-CH_2Cl_2 solution (1:3, v/v) to obtain a final concentration of 10% (w/w of chitosan) and stirred for 10 min until the oil phase mixture became transparent. Thereafter, the oil phase was added dropwise into the aqueous phase and sonicated for 5 min to form O/W emulsion. The volume ratio of O/W was

fixed at 1:5. Afterwards, a solution of quinoline derivatives (0.5%, w/v) as the modifying agents was poured into the O/W nanoemulsion dropwise to prepare the crosslinked chitosan–quinoline nanoparticles suspension. The crosslinked chitosan nanoparticles solution was then centrifuged at 16,000 rpm for 30 min at 20 °C. Finally, the obtained chitosan–quinoline nanoparticles were washed well with deionized water and freeze–dried for 12 h. The blank chitosan–quinoline nanoparticles prepared similarly without adding of quercetin.

2.6 Drug loading and encapsulation efficiency

The encapsulation efficiency (EE) and loading capacity (LC) of quercetin loaded in chitosan–quinoline nanoparticles were determined by centrifugation of the drug–loaded chitosan–quinoline nanoparticles at 16,000 rpm for 30 min to remove the non–entrapped quercetin. The clear supernatant was analyzed to measure the ultraviolet absorbance by using a UV–vis spectrophotometer at 373 nm. EE and LC were thus estimated from Eqs. (1) and (2), respectively:

$$\text{EE}\ (\%) = \frac{\text{QCt}-\text{QCf}}{\text{QCt}} \times\ 100 \qquad (1)$$

$$\text{LC}\ (\%) = \frac{\text{QCt}-\text{QCf}}{\text{Weight of nanoparticles}} \times\ 100 \qquad (2)$$

Where QCt is the total amount of quercetin used in the preparation of nanoparticles and QCf is the free quercetin present in the supernatant.

2.7 *In vitro* quercetin release

The quercetin release profile of the chitosan–quinoline nanoparticles was carried by a dialysis method. Typically, the weighed freeze–dried quercetin–loaded chitosan–quinoline nanoparticles were dispersed in release medium (phosphate buffer saline (PBS), pH 7.4 and pH 5.8) with a concentration of 1 mg/mL at a membrane dialysis bag (cut off 12,000 kDa).

The end–sealed dialysis bag was suspended into a container with 10 mL of PBS at the same pH value as that in the bag. The outer phase of the release media was maintained at 37 ± 0.5 °C with continuous stirring at a speed of 50 rpm. At prescheduled time intervals, 5 mL of samples were withdrawn in both of pH medium and replaced with an equal volume of fresh media to maintain a constant volume. The cumulative amount of quercetin released from chitosan–quinoline nanoparticles in each buffer was determined by measuring the absorbance at 373 nm in a UV–vis Spectrophotometer. To identify the mechanism for the release of quercetin from crosslinked and non-crosslinked chitosans, the suitability of Higuchi [31] and Korsmeyer–Peppas [32] equations were evaluated according to the following equations (Equations 3 and 4, respectively):

$$\frac{M_t}{M_\infty} = k\sqrt{t} \qquad (3)$$

$$\frac{M_t}{M_\infty} = k' t^n \qquad (4)$$

Where, Mt is cumulative amounts of released drug at time t and M∞ is cumulative amounts of released drug at infinite time. K and k' are Higuchi and Korsmeyer–Peppas constant. In the case of rod shape polymeric vehicles, n values that is used as release mechanism characterization are listed in **Table 1**.

Table 1. Diffusion exponent and solute release mechanism for rod shape matrices

Diffusion exponent (n)	Overall solut diffusion mechanism
n<0.45	Fickian diffusion
0.43<n<0.89	Anomalous (non- Fickian) diffusion
0.89<n<1	Case II transport
n>1	Super case II transport

2.8 *In vitro* cytotoxicity evaluation

MTT assay using HeLa cell lines was employed for determination of the *in vitro* cytotoxicity of free quercetin and the quercetin–loaded chitosan–quinoline nanoparticles. Typically, HeLa cells were seeded into 96–well plates at the density of 1.25×10^4 cells per well in 180 μL DMEM and then incubated in humidified incubator of 5% CO_2 at 37 ℃ for 24 h. After that, the medium was replaced by fresh corresponding medium containing solutions of pure quercetin and drug–loaded chitosan–quinoline nanoparticles at concentrations of 10 to 400 μg mL^{-1}. After incubated for 48 h, 20 μL of MTT solution (5 μg mL^{-1} in PBS) was added to every well and the cells were incubated for another 4 h. The medium containing MTT was then removed, and displaced by 150 μL of dimethyl sulphoxide (DMSO) per well for 10 min at ambient temperature to dissolve the formazan crystals. Finally, the absorbance of the solution was measured at a wavelength of 570 nm using a microplate reader and the relative cell viability (%) was calculated by the following equation:

$$\text{Cell viability (\%)} = \frac{\text{Abs (test cell)}}{\text{Abs (controlled cell)}} \times 100\% \quad (3)$$

2.9. Optical Microscopy Analysis

HeLa cells were cultured in 24-well plates at a density of 1×10^4 cells per well. After 24 h of incubation, cells were incubated without nanoparticles as control or with different concentration (100, 200 and 400 μg/mL) of two types of chitosan nanorods for 4 h at 37 °C. After that, morphologies of the cells were observed using an optical microscope.

3. Results and discussion

3.1 Design, synthesis and characterization

CFQ and FQO were prepared according to the procedure previously reported [30,33] as the modifying agents for the preparation of chitosan–quinoline nanoparticles. The synthetic routes are presented in **Scheme 1**. CFQ was synthesized starting from acetanilide via a Vilsmeier–Haack reaction. Subsequently, heating CFQ in aqueous acetic acid at reflux led to FQO in good yield (93%). All spectral data including IR, ^{1}H NMR and Mass of 2-chloro-3-formylquinoline and 3-formylquinolin-2(1*H*)-one were consistent with those of authentic samples.

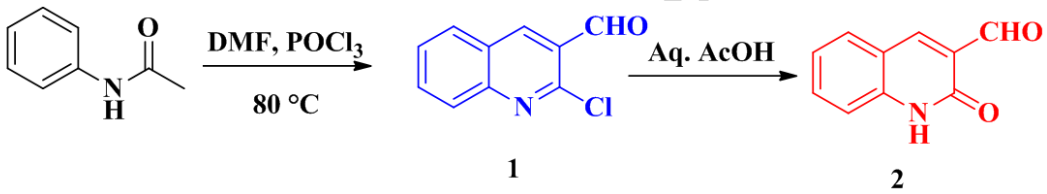

1 2

Scheme 1. Synthesis of CFQ e and FQO

The ^{1}H NMR spectrum of CFQ revealed characteristic signals at δ 10.52 (s, 1H) and 7.61-8.04 (m, 5H) due to the aldehyde and aromatic protons, respectively (**Figure 1A**).

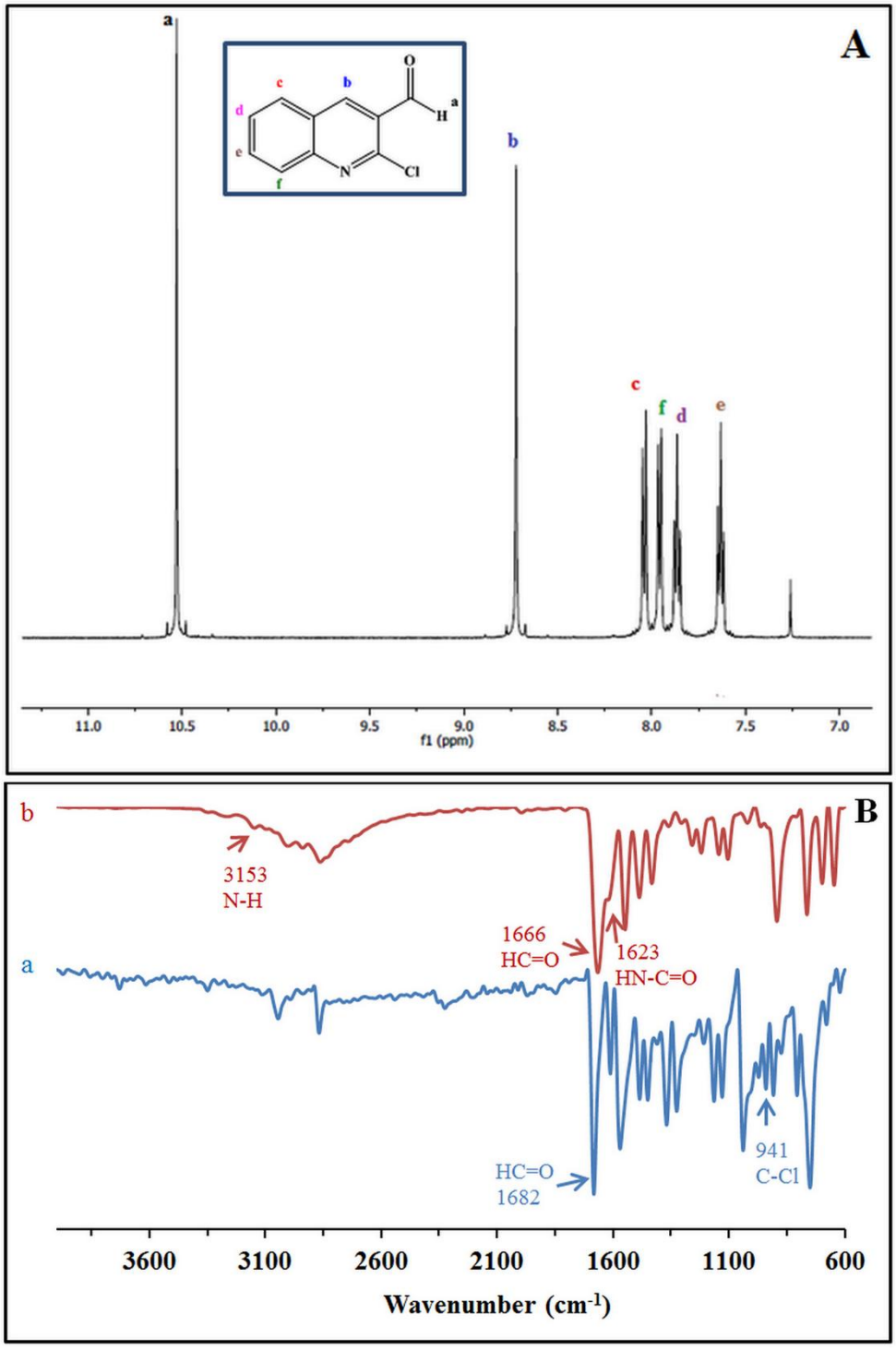

Figure 1. (A) ^{1}H-NMR spectra of CFQ and (B) FT-IR spectra of CFQ (a) and FQO (b)

Similarly, the appearance of signals at δ 10.27-10.48 (brs, 1H), 10.63 (s, 1H) and 7.72-8.76 (m, 5H) due to the NH, aldehyde and aromatic protons in the ^{1}H NMR spectrum of FQO is consistent with the suggested structure (**Figure S3**). The IR spectrum of CFQ exhibited the

main signals at 1682 cm^{-1} and 941 cm^{-1} for C=O and C–Cl, respectively. The most prominent signals in the IR spectrum of FQO corresponded to the intense absorption bands at 3153 and 1666–1623 cm^{-1} attributed to the amide NH and carbonyl groups together with the disappearance of signal at 941 cm^{-1} for C–Cl absorption (**Figure 1B**).

The chitosan–quinoline nanoparticles were prepared by Schiff base reaction of the chitosan chains amine and the quinoline aldehyde groups (**Scheme 2**). Moreover, the chitosan–quinoline nanoparticles are further stabilized through the formation of hydrogen bonding between FQO amide groups. This in turn enhances the physicochemical properties of chitosan–quinoline network. On the other hand, because of the biological activity of quinoline compounds and their non-toxicity properties, it is expected that the incorporation of quinoline into chitosan polymer furnishes novel nanoparticles with modified biological activity.

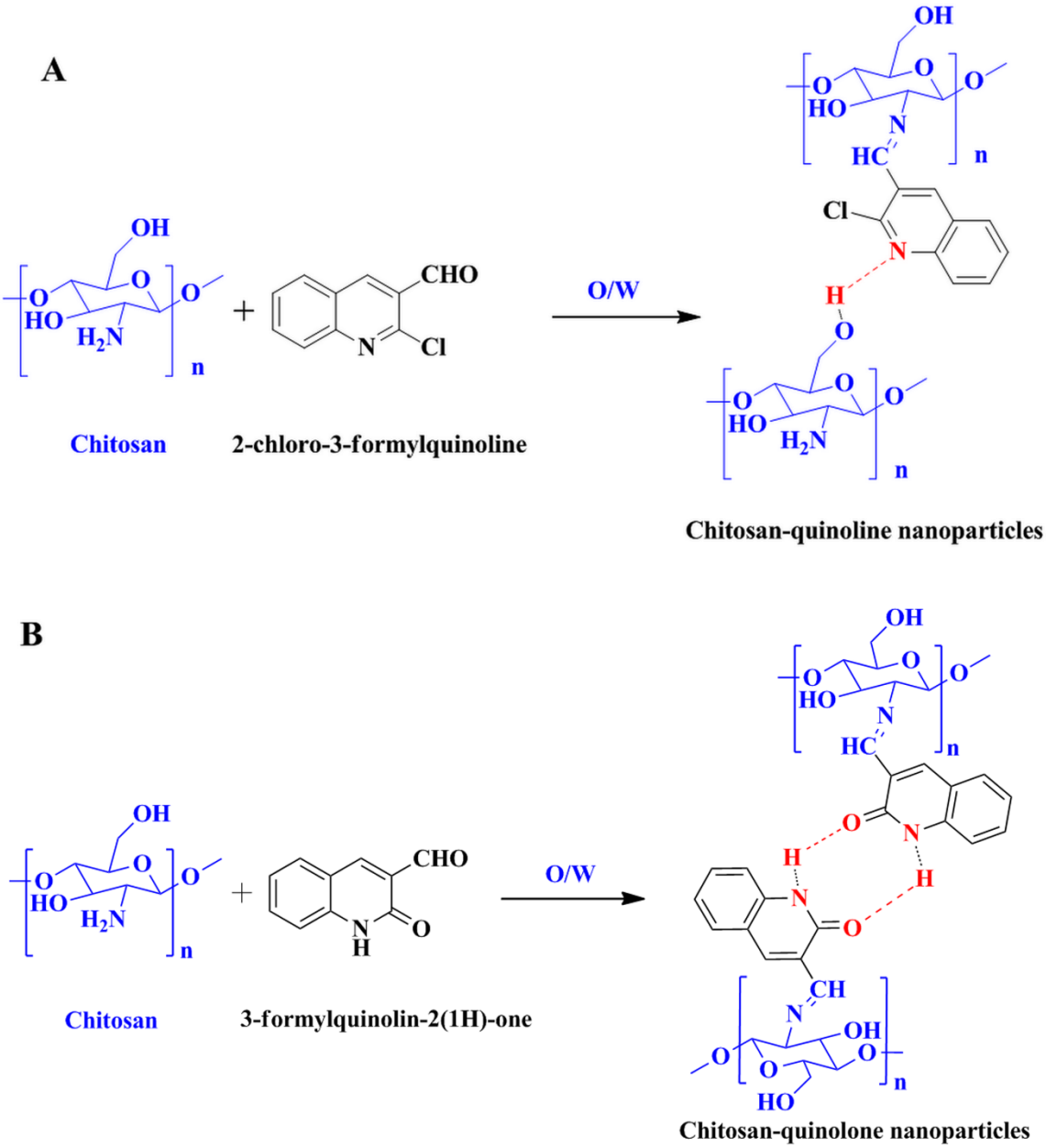

Scheme 2. Synthesis of chitosan–quinoline nanoparticles modified with CFQ (A) and with FQO (B)

The FT–IR spectra of pure chitosan and chitosan–quinoline nanoparticles are presented in **Figure 2**. The pure chitosan spectrum reveals the absorption peaks in 3200–3600, 3425 and 2873 cm^{-1} due to the intra– and intermolecular different –OH hydrogen bonds, N–H/O–H, and C–H stretching vibrations, respectively. Whereas other characteristic peaks of chitosan appears at 1654, 1592 and 1375 cm^{-1} are assigned to the amide I C=O, amide II NH

and amide III NHCO stretching vibrations, respectively, the broad peak displayed at 1025 cm^{-1} was attributed to the C–O absorption [34,35].

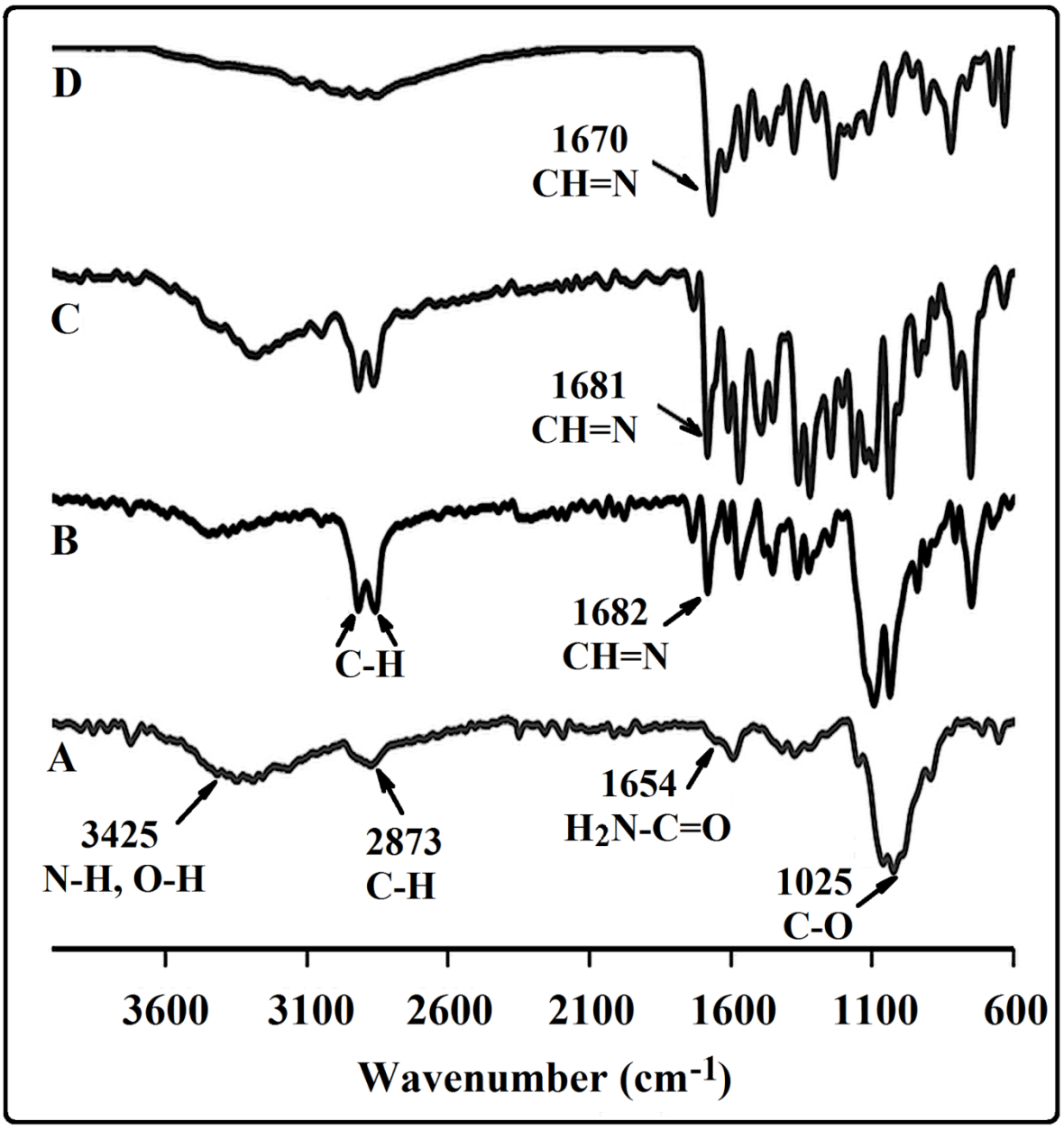

Figure 2. FT-IR spectra of the pure chitosan (A), blank chitosan–quinoline nanoparticles (B) and drug-loaded chitosan–quinoline nanoparticles crosslinked with CFQ (C) and FQO (D)

Compared to the pure chitosan, the strong absorption peaks observed at 1682 and 1670 cm^{-1} in the spectrum of the chitosan–quinoline nanoparticles due to C=N stretching vibrations indicate that imine bond formation has occurs via a chemical modification between the

chitosan chains amine and quinoline aldehyde groups [36,37]. Other specific peaks displayed at 752, 815, 1451 and 1612 cm^{-1} are attributed to the quinoline aromatic ring. Finally, observation of an increase in the absorptions at 2864 and 2918 cm^{-1} concomitant with the omission of absorbance at 2000–3900 cm^{-1} is significant, perhaps due the formation of chitosan–quinoline nanoparticles.

The XRD spectrum of pure chitosan presented in Figure 3A revealed the two broad peaks at $2\theta = 12$ and 20° in the former and in agreement with the previous reports [38]. In the XRD patterns of drug–loaded chitosan–quinoline nanoparticles, diffractive region is observed at 2θ of 16, 22, 29, 36, 39, 43, 47, and 48°. Observation of higher intensity in the XRD pattern of drug–loaded chitosan nanoparticles crosslinked with quinoline derivatives indicates their more crystalline structure. As such, it can be concluded that chemical modification with quinoline derivatives has converted the amorphous chitosan nanoparticles into a crystalline form.

The UV–vis absorption spectra of pure chitosan and chitosan–quinoline particles at 25 °C are shown in **Figure 3B**. Whereas the UV–vis absorption spectrum of pure chitosan is transparent and shows only a weak absorption band at 224 nm, those for chitosan–quinoline particles indicate two maxima at 250 and 306 nm due to the existence of $\pi \rightarrow \pi^*$ and $n \rightarrow \pi^*$ transitions of the azomethine chromophore moiety and quinoline heterocyclic ring. In addition, the UV–vis absorption spectrum of chitosan particles crosslinked with FQO exhibited a broad absorption band between the 360–450 nm regions, which could be assigned to the amide delocalized π-bond.

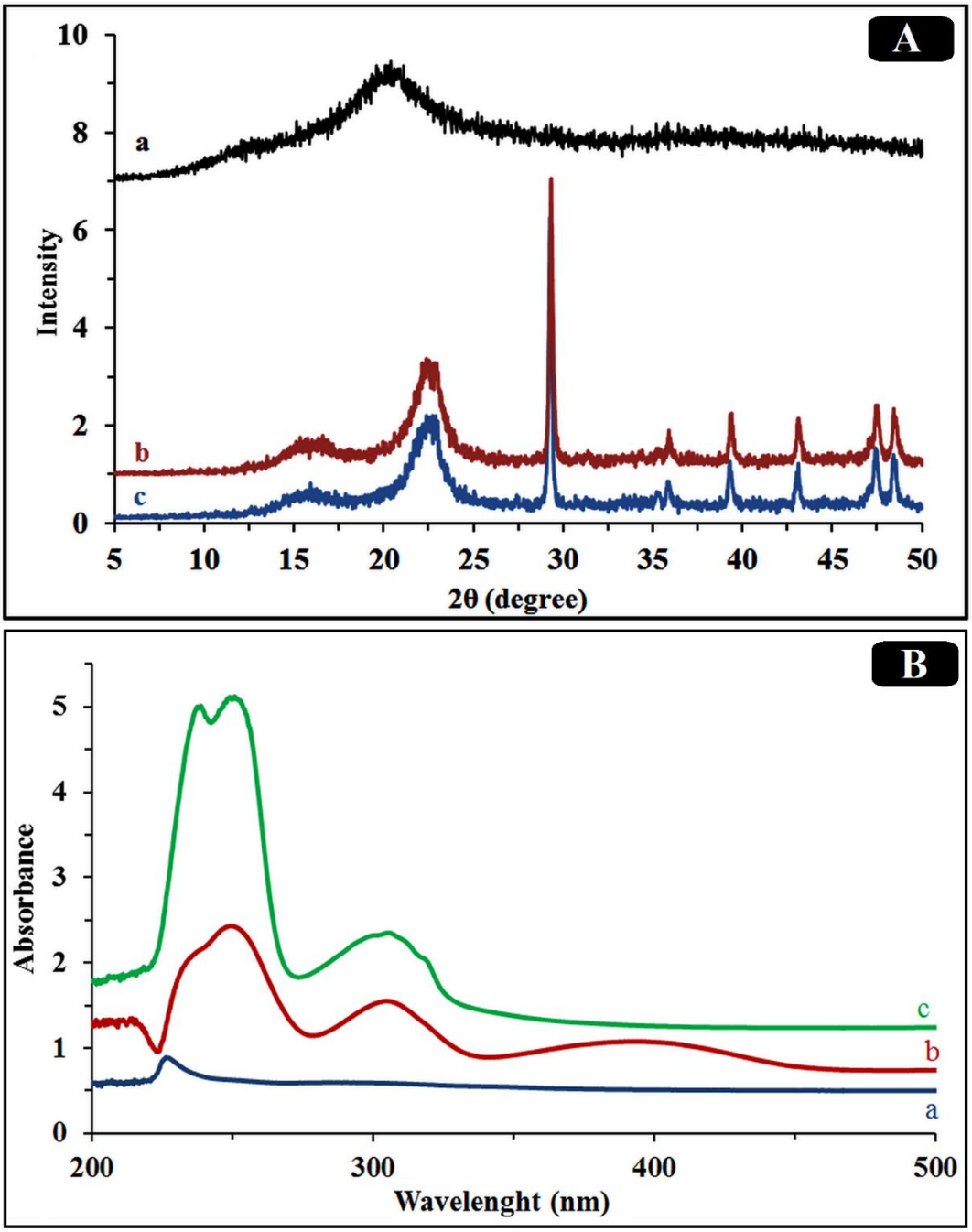

Figure 3. A: XRD patterns of chitosan powder (a), drug–loaded chitosan nanoparticles crosslinked with FQO (b) and drug–loaded chitosan nanoparticles crosslinked with CFQ (c). **B:** UV-Vis spectra of the pure chitosan (a), chitosan nanoparticles crosslinked with FQO (b) and chitosan nanoparticles crosslinked with CFQ (c).

The particle size of the chitosan–quinoline nanoparticles was determined by dynamic light scattering (DLS) technique. Because of the adhesion property of chitosan in aqueous solution, the nanoparticles tend to produce aggregates, which lead to an increase in their

average hydrodynamic diameter [39]. The progressive dispersion of the nanoparticles in aqueous suspension has been suggested as an efficient method of decreasing the inter–particle interactions [40] and utilized in this research. As indicated in **Figure 4A** and **B**, the average diameter of 150.7 nm with a zeta potential of −2.4 mV of blank chitosan nanoparticles crosslinked with CFQ changes to 174.8 nm with a zeta potential of −10.8 mV upon loading of quercetin. Accordingly, the average diameter of 141.2 nm with a zeta potential of −5.7 mV of the blank chitosan nanoparticles crosslinked with FQO also changes to 165.1 nm with a zeta potential of −14.1 mV upon loading of quercetin (**Figure 4C and D**). As such, the suitability of the chitosan–quinoline nanoparticles with negative zeta potential values as a drug delivery system is concluded.

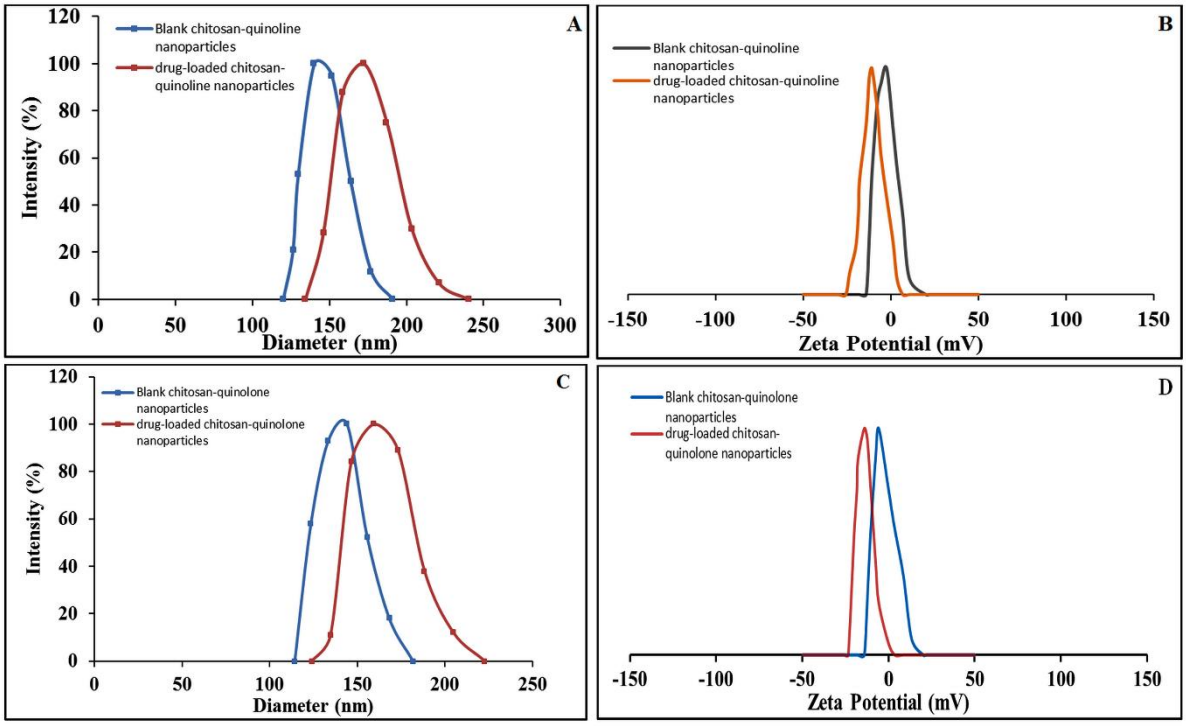

Figure 4. DLS results of chitosan nanoparticles crosslinked with CFQ (A) and FQO (C), and their zeta potential results: CFQ (B) and FQO (D)

The characterization of morphology and topography of the chitosan–quinoline nanoparticles was carried out using SEM and AFM techniques. The SEM images of blank and quercetin–loaded chitosan nanoparticles crosslinked with quinoline derivatives presented in **Figure 5** reveals that the blank chitosan–quinoline nanoparticles have spherical shape and nanosize structure, also reveal nearly uniform distribution with no intense particle agglomeration.

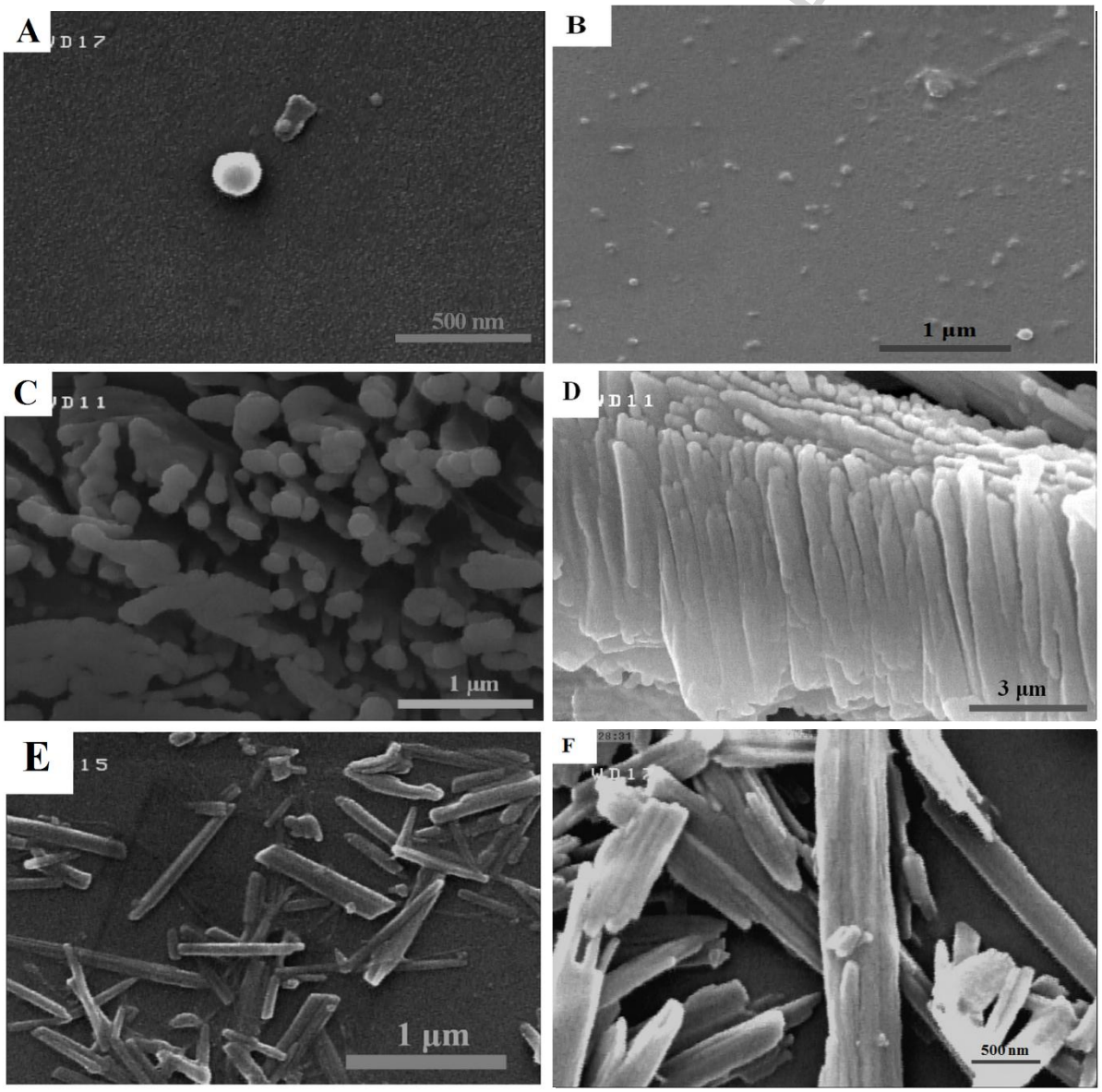

Figure 5. SEM images of the blank chitosan nanoparticles crosslinked with CFQ (A), crosslinked with FQO (B), drug-loaded chitosan nanoparticles crosslinked with CFQ (upper surface (C) and side surface (D)) and crosslinked with FQO (E) and (F)

The morphology of quercetin–loaded chitosan nanoparticles crosslinked with CFQ is a monolithic structure with a kind of pattern and the morphology of quercetin–loaded chitosan nanoparticles crosslinked with FQO is nanorod structure along with uniformity in size (**Figure 5C-F**). Differences in the morphology of the blank chitosan–quinoline nanoparticles and quercetin–loaded chitosan–quinoline nanoparticles can be attributed to the intermolecular hydrogen bonding and π–π (π–stacking) interactions present between quercetin and quinoline derivatives (**Scheme S1**).

In addition, AFM topographic images and 3D models of the surface topography (**Figure 6**) confirmed the nanorod-like morphology and nearly homogenous structure of quercetin–loaded chitosan nanoparticles made by crosslinking with quinoline derivatives, in agreement with SEM observations. The rod–like nanoparticles exhibited the enhanced cell adhesion, improved cell proliferation and transfection of living cells via their higher surface areas, with more effective penetration in tumors in comparison to those of spherical analogues [41]. Therefore, the quercetin–loaded chitosan nanoparticles crosslinked with quinoline derivatives having such surface morphology is favored for use in biomedical applications, especially drug delivery systems.

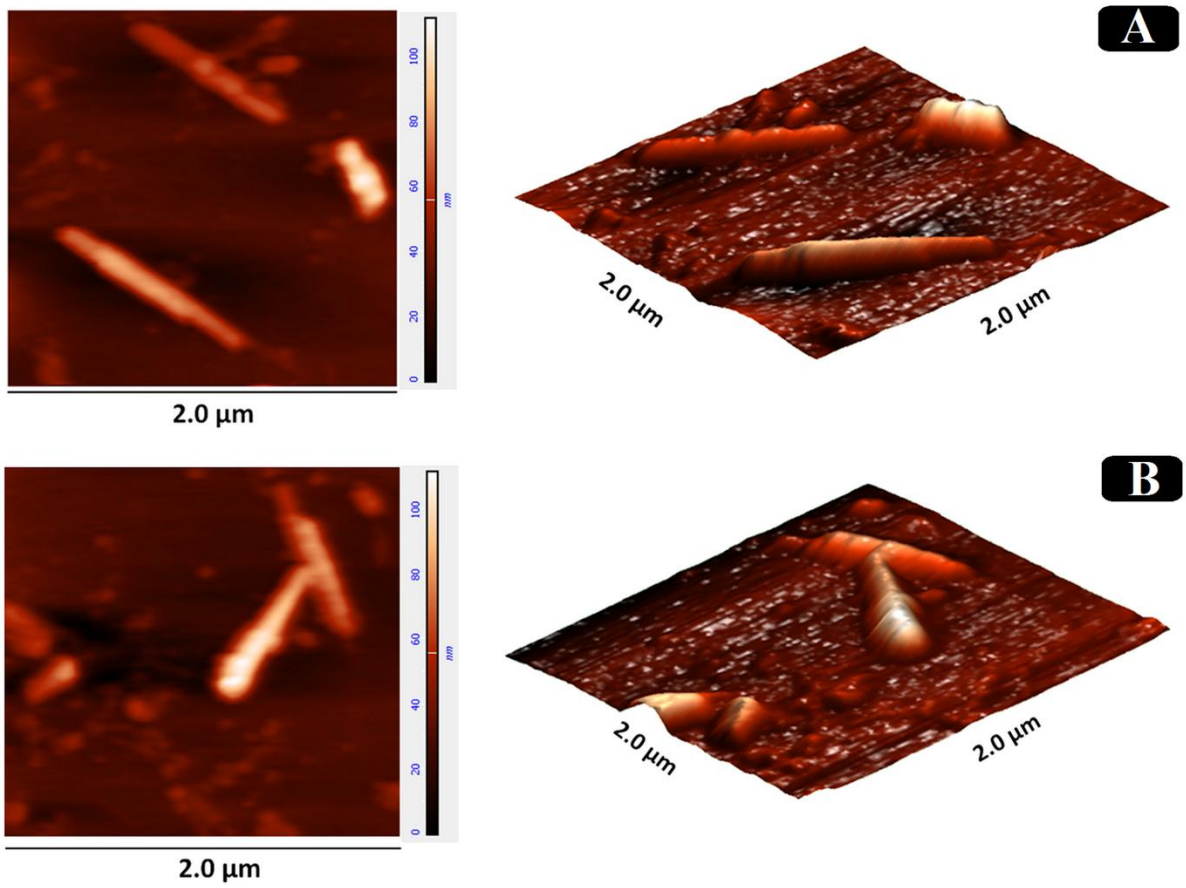

Figure 6. AFM images (2D) and (3D) of drug-loaded chitosan nanoparticles crosslinked with CFQ (A) and drug-loaded chitosan nanoparticles crosslinked with FQO (B)

3.2 Drug loading capacity and in vitro release profile

Quercetin, a potent and hydrophobic anticancer drug, was employed to measure the drug loading and release profile of the chitosan–quinoline nanoparticles. Low encapsulation efficiency was not expected due to the hydrophobic and π–π (π–stacking) interactions as well as intermolecular hydrogen bonding present between quercetin and the crosslinked chitosan nanoparticle quinoline groups. Accordingly, the drug LC and EE of the chitosan nanoparticles crosslinked with FQO determined as 9.6% and 77.2%, respectively, were higher than those of 4.8% and 65.8% found for chitosan nanoparticles crosslinked with CFQ. These efficiencies are higher than that found for quercetin-loaded chitosan nanoparticles modified with glycyrrhetinic acid [42]. The encapsulation efficiency depends on several parameters and one of the most important ones is the strong affinity between hydrophobic

drug and hydrophobic domains in nanocarrier. It was found that this hydrophobic domains in chitosan could be obtained by adding hydrophobic co-materials to the carrier formulation, like lecithin [43], or pre-adhering of quercetin to carriers before particle crosslinking [44]. In this report, we used the former method, by inserting aromatic crosslinkers in the structure of chitosan. Consequently, a larger amount of quercetin preferred to encapsulate in nanocarriers during nanoparticle formation process. However, these interactions may reduce the diffusion of quercetin from nanocarriers during the release process. On the other hand, the low solubility of quercetin in water, automatically forced the drug molecules to attract to the surface or outer layers of nanoparticle and enhance its encapsulation efficiency. But, afterward, a complete release of drug in short period of time is observable in these systems. These results exhibit the improved stability of the quercetin–loaded chitosan nanoparticles crosslinked with FQO. The quercetin release profile of the chitosan–quinoline nanoparticles and chitosan nanoparticles without using quinoline derivatives in response to pH values of 7.4 and 5.8 was studied in a dialysis setup at 37 °C. Based on the *in vitro* release profile, it was found that the chitosan nanoparticles crosslinked with quinoline derivatives release quercetin much faster at pH 5.8 than that of pH 7.4. In acidic environment at low pH value (pH < 6), the amino groups of chitosan are protonated and positively charged, so its intramolecular electrostatic repulsion and hydrophilicity enhancement make chitosan nanoparticles swell dramatically. By protonation of chitosan amino groups, the Schiff base bonding becomes instable and decomposition of the crosslinkers occurred. Therefore, by using such a reversible crosslinking reaction between chitosan and 2-chloro-3-formylquinoline and 3-formylquinolin-2(1H)-one, an interesting pH-responsive controlled release process can be achieved for acid-triggered burst release with the proposed microcapsule. As shown in **Figure 7**, the burst release of chitosan nanoparticles crosslinked with FQO and CFQ is 69.3% and 78.4%, at pH 5.8 during the first 8 h, respectively. The

quercetin release mechanism at this step could be illustrated by the quercetin diffusion localized at the surface of the chitosan–quinoline nanoparticles [45,46]. On the other hand, the cumulative release of chitosan–quinoline and chitosan–quinolone nanoparticles at pH 7.4 is 56.4% and 52.7% in first 8 h, respectively. After 150 h, whereas the drug release of chitosan nanoparticles crosslinked with CFQ was approximately completed at pH 5.8, only 82% of drug release occurred from chitosan nanoparticles crosslinked with FQO under similar condition. This could be explained by the stronger intermolecular hydrogen bonding between quercetin and FQO, which caused the lower release rate in comparison with chitosan nanoparticles crosslinked with CFQ.

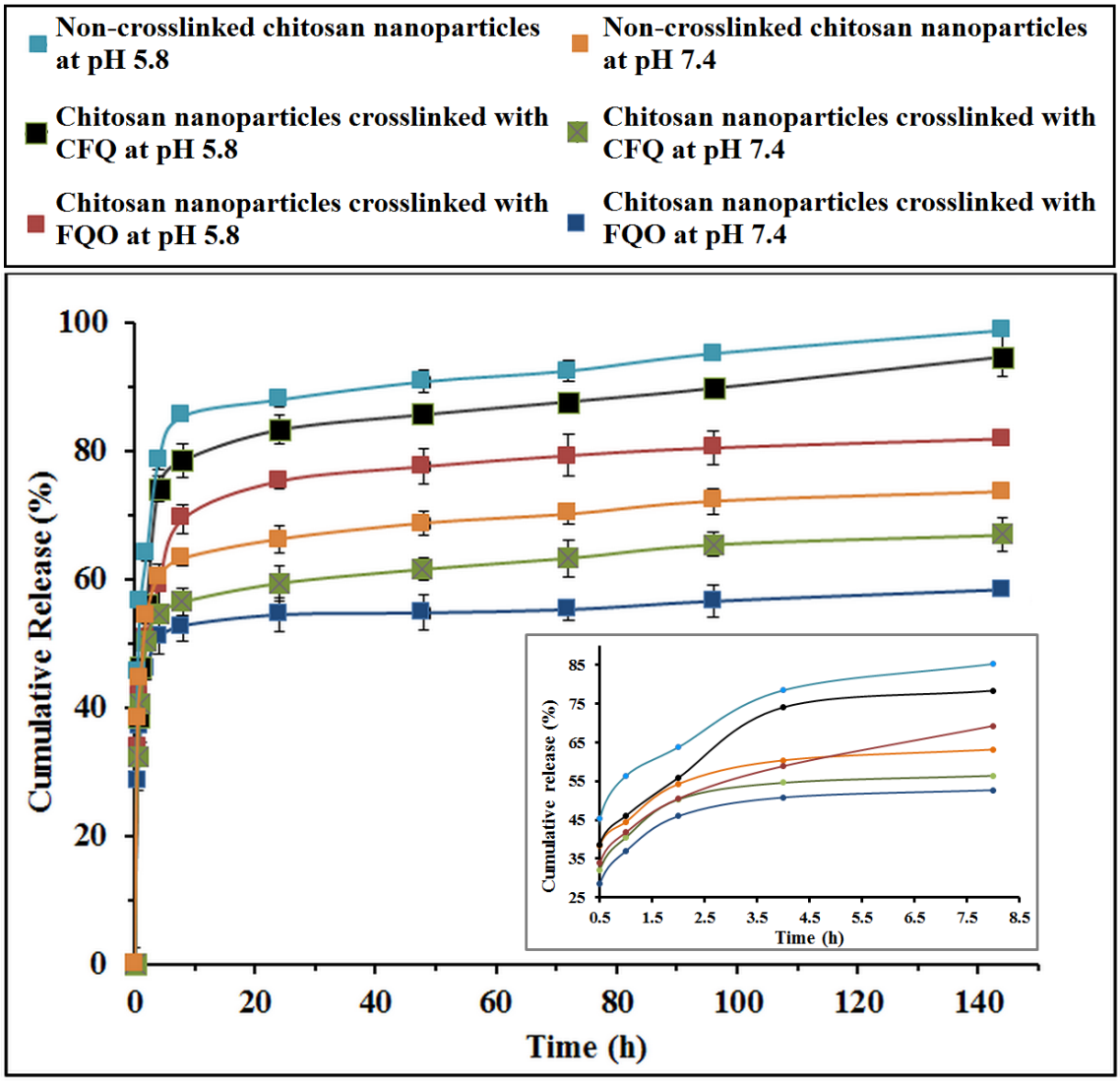

Figure 7. *In vitro* release of quercetin from drug-loaded chitosan nanoparticles in PBS under different pH conditions (The inset shows the results for the first 10 hours.)

Mechanism of drug release from crosslinked and non-crosslinked chitosan were analyzed at two pHs by Higuchi and Korsmeyer-peppas equations and their data were listed in **Table 2**. Higuchi's release rate constant (k) and its correlation coefficient values (r^2) were determined. The release data was also fitted into Korsmeyer–Peppas model and by considering release rate constants (k') and release constants (n), the fitting accuracy was calculated using correlation coefficient values (r^2). When comparing these two model, the best fit method is Korsmeyer–Peppas, regarding to highest values of correlation coefficients, accordingly, the release mechanisms for all samples at both pHs are Fickian diffusion.

Table 2. Estimated values obtained by fitting the drug release data to the Higuchi and Korsmeyer-Peppas models

Chitosan nanorods	pH	Higuchi		Korsmeyer-peppas			Release mechanism
		k	r^2	k'	r^2	n	
Crosslinked with FQO	7.4	0.1866	0.8156	0.8109	0.9076	0.2213	Fickian diffusion
Crosslinked with CFQ		0.1735	0.7668	0.7974	0.9045	0.2060	Fickian diffusion
Non-crosslinked		0.1610	0.8795	0.8073	0.9546	0.1887	Fickian diffusion
Crosslinked with FQO	5.8	0.2017	0.9763	0.5040	0.9957	0.2568	Fickian diffusion
Crosslinked with CFQ		0.2116	0.9338	0.7334	0.9980	0.2598	Fickian diffusion
Non-crosslinked		0.1916	0.9470	0.7741	0.9816	0.2306	Fickian diffusion

The SEM images of quercetin–loaded chitosan nanoparticles crosslinked with quinoline derivatives at pH 7.4 and 5.8 presented in **Figure 8**. In neutral medium (pH 7.4), the quercetin–loaded chitosan nanoparticles crosslinked with quinoline derivatives maintain good nanorod shape and structural integrity, which promises that quercetin localized at the matrix of the chitosan–quinoline nanoparticles would not be released before reaching the tumor cells. While, in acidic medium (pH 5.8), the quercetin–loaded chitosan–quinoline nanoparticles have lost their nanorod shape and converted into tiny nanocubic crystals and

consequently their disposal of the body is more easily. With the protonation of the chitosan amine groups at low pH, the imine bonds between the chitosan chains and quinoline molecules becomes weaken and instable, which led to decomposition of the crosslinked chitosan nanoparticles and quercetin was eventually released very rapidly. Therefore, by utilization of such a reversible crosslinking reaction between chitosan and quinoline derivatives, an interesting pH-sensitive controlled release system can be achieved.

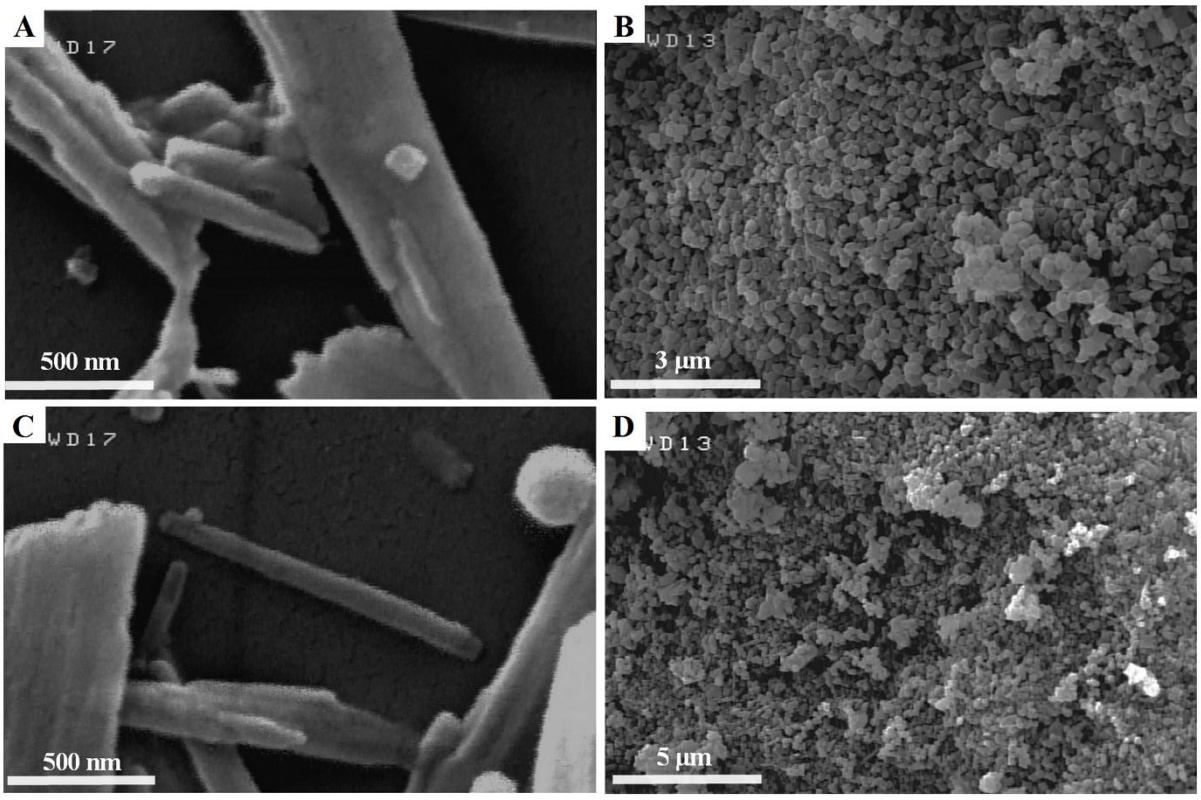

Figure 8. SEM images of quercetin-loaded chitosan nanoparticles crosslinked with CFQ in pH 7.4 and 5.8 (A) and (B) respectively, quercetin-loaded chitosan nanoparticles crosslinked with FQO

3.3 Cell viability assays

MTT assay was used to evaluate the *in vitro* cytotoxicity of quercetin–loaded chitosan–quinoline nanoparticles, quercetin–loaded chitosan nanoparticles without of modification with quinoline derivatives, CFQ, FQO and the free quercetin at different concentrations from 10 to 400 μg mL^{-1}, using HeLa cells as model. All the formulations exhibited remarkable

anticancer activity against HeLa cells after 48 h incubation. As shown in **Figure 9**, as the concentration of quercetin increased, the cell viability was further reduced. The half maximal inhibitory concentration (IC_{50}) value of the chitosan nanoparticles crosslinked with CFQ and FQO and free quercetin against HeLa cell lines were 10, 14 and about 32 μg mL^{-1}, respectively. These results showed that quercetin–loaded chitosan–quinoline nanoparticles reveal higher cytotoxicity for cancer cell proliferation in comparison to that of free quercetin and quercetin–loaded chitosan nanoparticles without of modification with quinoline derivatives. Significantly, no remarkable difference was observed in cell viability between the quercetin–loaded chitosan nanoparticles crosslinked with quinoline derivatives during the experiment. Therefore, it can be concluded that chitosan–quinoline nanoparticles are able to enter the cells and show favorable pharmacological effect on cancer cells. Beside the anticancer activity of drug-loaded chitosan nanorods with two crosslinkers, the higher cell viability of non-crosslinked sample despite its higher drug release is interesting. In fact, after internalization of crosslinked nanoparticles by cancer cells, in the acidic media of lysosome and endosome the imine linkages of quinoline crosslinkers were quickly cleaved to protonated amino groups. This positive charge encourages nanoparticles to endosome/lysosome escape, which in turn provides the opportunity to increase system circulation efficiency and enhance favorable cellular and subcellular bioavailability [47].

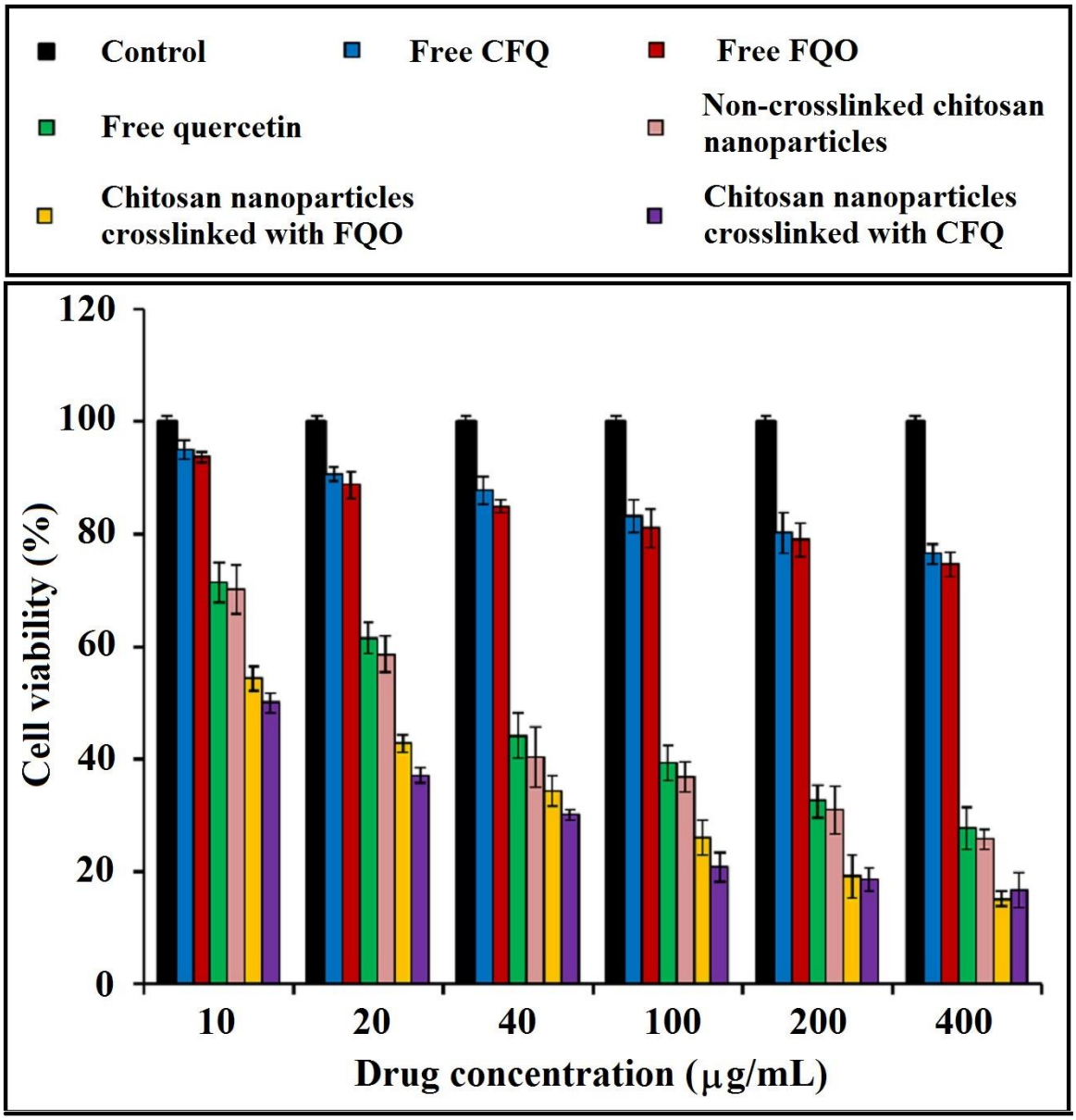

Figure 9. Cell viability (%) of HeLa cancer cells after incubation with different quercetin formulations for 48 h

Optical microscopy was employed to examine the influences of different concentration of two kinds of crosslinked chitosan nanoparticles on the morphology of HeLa cells. It can be seen from **Figure 10**, that the cells which were incubated with drug-loaded nanorods even after 4 hours incubation could change the spindle-like morphology of untreated cell (control cells) to rounded one. On the other hand, the images of HeLa cells incubated with higher concentrations of NPs show an increase in internalization, the presence of nanoparticles

inside the cells is the evidence of this phenomena. A homogeneous distribution of NPs inside the cells is also noteworthy.

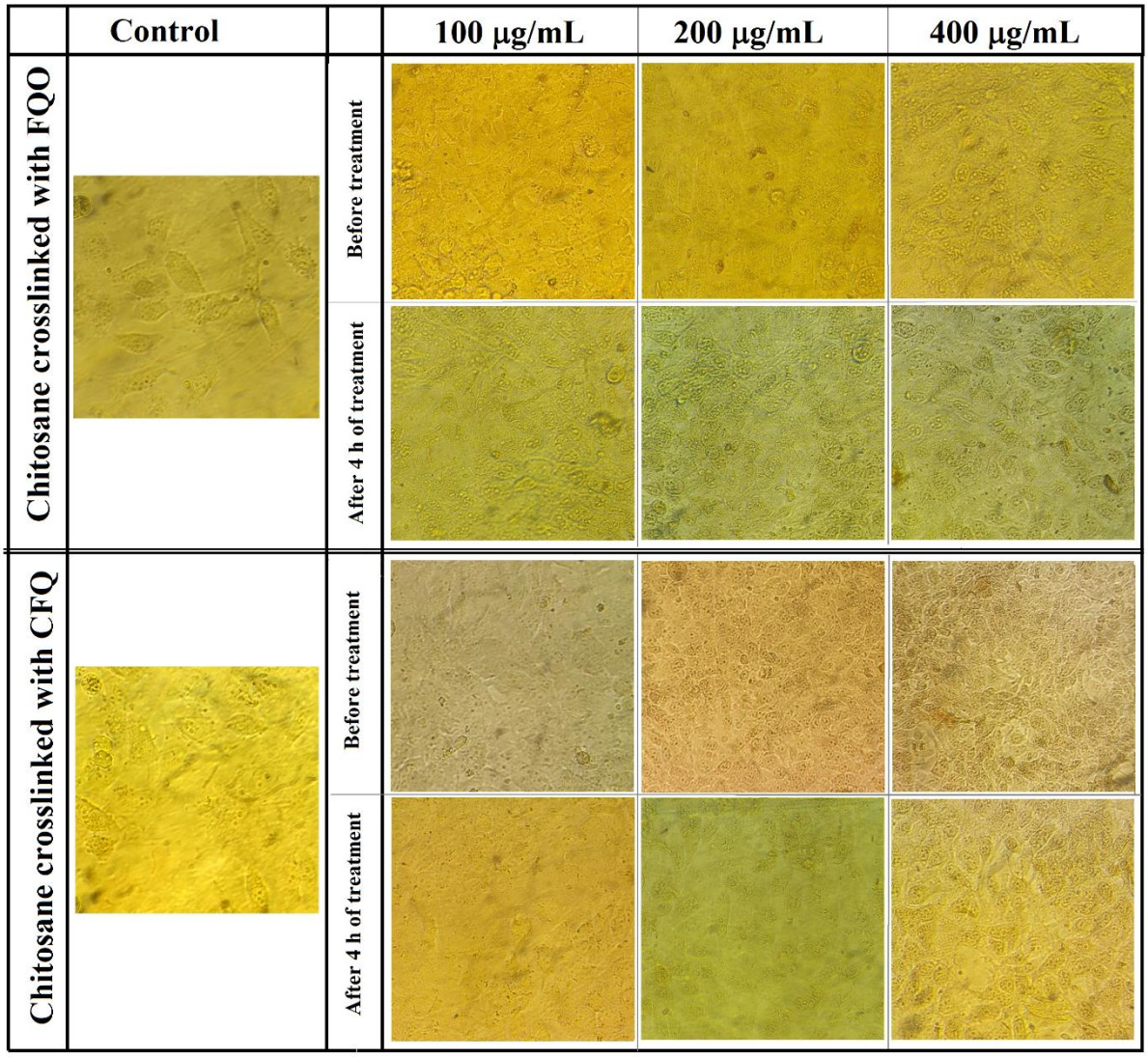

Figure 10. Optical microscopy images of HeLa cells incubated with different concentrations of chitosan crosslinked with quinoline derivatives: before treatment and after 4h of treatment

4. Conclusions

In summary, novel rod–like drug–loaded chitosan–quinoline nanoparticles were successfully designed and synthesized via an oil–in–water nanoemulsion method, using 2-chloro-3-formylquinoline and 3-formylquinolin-2(1*H*)-one as friendly and non-toxic crosslinking agents. The structures of the obtained nanoparticles were carefully studied. The

chitosan–quinoline nanoparticles were used as nanocarriers for efficient encapsulation of quercetin, exposing a pH–sensitive controllable release. The nanoparticles showed particle size in the range of 141–174 nm. The morphology of quercetin–loaded chitosan nanoparticles crosslinked with CFQ and FQO was a monolithic structure with a kind of pattern and a regular nanorod shape, respectively. Due to the cleavage of crosslinked imine linkages present between chitosan and quinoline derivatives, the in vitro results displayed an accelerated drug release at lower pH condition in comparison to that occur under physiological conditions. Moreover, the in vitro quercetin release data showed that the chitosan nanoparticles crosslinked with FQO displayed a slow drug release in comparison to that of chitosan nanoparticles crosslinked with CFQ. In addition, the SEM images of quercetin–loaded chitosan nanoparticles crosslinked with quinoline derivatives in acidic medium exhibited that nanoparticles have lost their nanorod shape and converted into tiny nanocubic crystals, which led to decomposition of the crosslinked chitosan nanoparticles and quercetin was eventually released very rapidly. Compared to free quercetin, the quercetin–loaded chitosan–quinoline nanoparticles showed impressive comparable cytotoxicity against HeLa cells. Based on the obtained results, utilization of this new type of chitosan nanoparticles crosslinked with quinoline derivatives as potential drug delivery systems is concluded.

References

[1] M.R. Kumar, R.A. Muzzarelli, C. Muzzarelli, H. Sashiwa, A. Domb, Chitosan chemistry and pharmaceutical perspectives, Chemical reviews 104 (2004) 6017-6084.

[2] D. Depan, P.V. Surya, B. Girase, R. Misra, Organic/inorganic hybrid network structure nanocomposite scaffolds based on grafted chitosan for tissue engineering, Acta biomaterialia 7 (2011) 2163-2175.

[3] M. Diaconu, S.C. Litescu, G.L. Radu, Laccase–MWCNT–chitosan biosensor—A new tool for total polyphenolic content evaluation from in vitro cultivated plants, Sensors and Actuators B: Chemical 145 (2010) 800-806.

[4] R. Jayakumar, D. Menon, K. Manzoor, S. Nair, H. Tamura, Biomedical applications of chitin and chitosan based nanomaterials—A short review, Carbohydrate Polymers 82 (2010) 227-232.

[5] S.F. Peng, M.J. Yang, C.J. Su, H.L. Chen, P.W. Lee, M.C. Wei, H.W. Sung, Effects of incorporation of poly (γ-glutamic acid) in chitosan/DNA complex nanoparticles on cellular uptake and transfection efficiency, Biomaterials 30 (2009) 1797-1808.

[6] Y.Q. Ye, F.L. Yang, F.Q. Hu, Y.Z. Du, H. Yuan, H.Y. Yu, Core-modified chitosan-based polymeric micelles for controlled release of doxorubicin, International journal of pharmaceutics 352 (2008) 294-301.

[7] M. Thanou, J.C. Verhoef, H.E. Junginger, Oral drug absorption enhancement by chitosan and its derivatives, Advanced drug delivery reviews 52 (2001) 117-126.

[8] Y.N. Fu, Y. Li, G. Li, L. Yang, Q. Yuan, L. Tao, X. Wang, Adaptive Chitosan Hollow Microspheres as Efficient Drug Carrier, Biomacromolecules 18 (2017) 2195-2204.

[9] L. Liu, J.P. Yang, X.J. Ju, R. Xie, Y.M. Liu, W. Wang, J.J. Zhang, C.H. Niu, L.Y. Chu, Monodisperse core-shell chitosan microcapsules for pH-responsive burst release of hydrophobic drugs, Soft Matter 7 (2011) 4821-4827.

[10] K. Gupta, F.H. Jabrail, Glutaraldehyde and glyoxal cross-linked chitosan microspheres for controlled delivery of centchroman, Carbohydrate research 341 (2006) 744-756.

[11] A.P. Rokhade, N.B. Shelke, S.A. Patil, T.M. Aminabhavi, Novel interpenetrating polymer network microspheres of chitosan and methylcellulose for controlled release of theophylline, Carbohydrate Polymers 69 (2007) 678-687.

[12] S. Rahimi, S. Khoee, M. Ghandi, Development of photo and pH dual crosslinked coumarin-containing chitosan nanoparticles for controlled drug release, Carbohydrate Polymers 201 (2018) 236-245.

[13] M.M. Iftime, S. Morariu, L. Marin, Salicyl-imine-chitosan hydrogels: Supramolecular architecturing as a crosslinking method toward multifunctional hydrogels, Carbohydrate Polymers 165 (2017) 39-50.

[14] J.P. Michael, Quinoline, quinazoline and acridone alkaloids, Natural product reports 16 (1999) 697-709.

[15] C.W. Wright, J. Addae-Kyereme, A.G. Breen, J.E. Brown, M.F. Cox, S.L. Croft, Y. Gökçek, H. Kendrick, R.M. Phillips, P.L. Pollet, Synthesis and evaluation of cryptolepine analogues for their potential as new antimalarial agents, Journal of Medicinal Chemistry 44 (2001) 3187-3194.

[16] S. Cretton, S. Dorsaz, A. Azzollini, Q. Favre-Godal, L. Marcourt, S.N. Ebrahimi, F. Voinesco, E. Michellod, D. Sanglard, K. Gindro, J.L. Wolfender, M. Cuendet, P. Christen, Antifungal quinoline alkaloids from Waltheria indica, Journal of natural products 79 (2016) 300-307.

[17] M. Alam, M. Shaharyar, H. Hamid, S. Nazreen, S. Haider, M.S. Alam, Synthesis of novel 8-hydroxy quinolin based 1, 3, 4-oxadiazoles and S-substituted 1, 2, 4-triazole derivatives and evaluation of their anti-inflammatory, analgesic, ulcerogenic and anti-microbial activities, Medicinal Chemistry 7 (2011) 663-673.

[18] R.E. Khidre, B.F. Abdel-Wahab and F.A. Badria, New quinoline-based compounds for analgesic and anti-inflammatory evaluation, Letters in Drug Design & Discovery 8 (2011) 640-648.

[19] S. Vandekerckhove, M. D'hooghe, Quinoline-based antimalarial hybrid compounds, Bioorganic & medicinal chemistry 23 (2015) 5098-5119.

[20] K. Plevová, K. Briestenská, F. Colobert, J. Mistríková, V. Milata, F.R. Leroux, Synthesis and biological evaluation of new nucleosides derived from trifluoromethoxy-4-quinolones, Tetrahedron Letters 56 (2015) 5112-5115.

[21] A. Kamal, R. Abdul, S. Riyaz, Y. Poornachandra, B. Moku, C.G. Kumar, S.M. Hussaini, B. Sridhar, P.K. Machiraju, Regioselective synthesis, antimicrobial evaluation and theoretical studies of 2-styryl quinolines, Organic & biomolecular chemistry 13 (2015) 1347-1357.

[22] Y. Parthasaradhi, S. Suresh, B.R. Kumar, T.S. Jyostna, Design and Synthesis of Some New Quinoline Based 1, 2, 3-Triazoles as Antimicrobial and Antimalarial Agents, Orbital: The Electronic Journal of Chemistry 7 (2015) 264-269.

[23] O. Afzal, S. Kumar, M.R. Haider, M.R. Ali, R. Kumar, M. Jaggi, S. Bawa, A review on anticancer potential of bioactive heterocycle quinoline, European journal of medicinal chemistry 97 (2015) 871-910.

[24] D.A. Ibrahim, D.A.A. El Ella, A.M. El-Motwally, R.M. Aly, Molecular design and synthesis of certain new quinoline derivatives having potential anticancer activity, European journal of medicinal chemistry 102 (2015) 115-131.

[25] R.S. Gonçalves, C.R. Kaiser, M.C. Lourenço, M.V. de Souza, J.L. Wardell, S.M. Wardell, A.D. Da Silva, Synthesis and antitubercular activity of new mefloquine-oxazolidine derivatives, European journal of medicinal chemistry 45 (2010) 6095-6100.

[26] M.H. Gelb, Drug discovery for malaria: a very challenging and timely endeavor, Current opinion in chemical biology 11 (2007) 440-445.

[27] D.S. Ongarora, J. Gut, P.J. Rosenthal, C.M. Masimirembwa, K. Chibale, Benzoheterocyclic amodiaquine analogues with potent antiplasmodial activity: Synthesis and pharmacological evaluation, Bioorganic & medicinal chemistry letters 22 (2012) 5046-5050.

[28] N. Sharma, D. Mohanakrishnan, U.K. Sharma, R. Kumar, A.K. Sinha, D. Sahal, Design, economical synthesis and antiplasmodial evaluation of vanillin derived allylated chalcones and their marked synergism with artemisinin against chloroquine resistant strains of Plasmodium falciparum, European journal of medicinal chemistry 79 (2014) 350-368.

[29] R. Abonia, D. Insuasty, J. Castillo, B. Insuasty, J. Quiroga, M. Nogueras, J. Cobo, Synthesis of novel quinoline-2-one based chalcones of potential anti-tumor activity, European journal of medicinal chemistry 57 (2012) 29-40.

[30] M.K. Singh, A. Chandra, B. Singh, R.M. Singh, Synthesis of diastereomeric 2, 4-disubstituted pyrano [2, 3-b] quinolines from 3-formyl-2-quinolones through O–C bond formation via intramolecular electrophilic cyclization, Tetrahedron Letters 48 (2007) 5987-5990.

[31] T. Higuchi, Mechanism of sustained-action medication. Theoretical analysis of rate of release of solid drugs dispersed in solid matrices, Journal of Pharmaceutical Sciences 52 (1963) 1145–1149.

[32] R.W. Korsmeyer, R. Gurny, E. Doelker, P. Buri, N.A. Peppas, Mechanisms of solute release from porous hydrophilic polymers, International Journal of Pharmaceutics 15 (1983) 25–35.

[33] M. Ghandi, S. Rahimi, N. Zarezadeh, Synthesis of novel tetrazole containing quinoline and 2, 3, 4, 9-tetrahydro-1H-β-carboline derivatives, Journal of Heterocyclic Chemistry 54 (2017) 102-109.

[34] H. Chen, X. Hu, E. Chen, S. Wu, D.J. McClements, S. Liu, B. Li, B. Li, Preparation, characterization, and properties of chitosan films with cinnamaldehyde nanoemulsions, Food Hydrocolloids 61 (2016) 662-671.

[35] S. Kumar, J. Koh, Physiochemical, circular dichroism-induced helical conformation and optical property of chitosan azo-based amino methanesulfonate complex, Journal of Applied Polymer Science 124 (2012) 4897-4903.

[36] S. Hirano, K. Nagamura, M. Zhang, S.K. Kim, B.G. Chung, M. Yoshikawa, T. Midorikawa, Chitosan staple fibers and their chemical modification with some aldehydes, Carbohydrate Polymers 38 (1999) 293-298.

[37] S. Noppakundilograt, P. Buranagul, W. Graisuwan, C. Koopipat, S. Kiatkamjornwong, Modified chitosan pretreatment of polyester fabric for printing by ink jet ink, Carbohydrate Polymers 82 (2010) 1124-1135.

[38] C. Demetgül, N. Beyazit, Synthesis, characterization and antioxidant activity of chitosan-chromone derivatives, Carbohydrate Polymers 181 (2018) 812-817.

[39] M.A. Pujana, L. Pérez-Álvarez, L.C.C. Iturbe, I. Katime, Biodegradable chitosan nanogels crosslinked with genipin, Carbohydrate Polymers 94 (2013) 836-842.

[40] P. Sorlier, C. Rochas, I. Morfin, C. Viton, A. Domard, Light scattering studies of the solution properties of chitosans of varying degrees of acetylation, Biomacromolecules 4 (2003) 1034-1040.

[41] S. Kumar, J. Koh, H. Kim, M. Gupta, P. Dutta, A new chitosan–thymine conjugate: Synthesis, characterization and biological activity, International journal of biological macromolecules 50 (2012) 493-502.

[42] H. Du, M. Liu, X. Yang, G. Zhai, The role of glycyrrhetinic acid modification on preparation and evaluation of quercetin-loaded chitosan-based self-aggregates. Journal of Colloid and Interface Science 460 (2015) 87-96.

[43] M.P. Souza, A.F.M. Vaz, M.T.S. Correia, M.A. Cerqueira, A.A. Vicente, M.G. Carneiro-da-Cunha, Quercetin-loaded lecithin/chitosan nanoparticles for functional food applications, Food and Bioprocess Technology 7 (2014) 1149–1159.

[44] W. Nan, L. Ding, H. Chen, F.U. Khan, L. Yu, X. Sui, X. Shi, Topical use of quercetin-loaded chitosan nanoparticles against ultraviolet B radiation, Frontiers in Pharmacology 9 (2018) 826.

[45] A. Jain, K. Thakur, P. Kush, U.K. Jain, Docetaxel loaded chitosan nanoparticles: Formulation, characterization and cytotoxicity studies, International Journal of Biological Macromolecules 69 (2014) 546-553.

[46] R. Yoksan, J. Jirawutthiwongchai, K. Arpo, Encapsulation of ascorbyl palmitate in chitosan nanoparticles by oil-in-water emulsion and ionic gelation processes, Colloids and Surfaces B: Biointerfaces 76 (2010) 292-297.

[47] A. Paillard, F. Hindré, C. Vignes-Colombeix, J.P. Benoit, E. Garcion, The importance of endo-lysosomal escape with lipid nanocapsules for drug subcellular bioavailability, Biomaterials 31(2010) 7542-54.

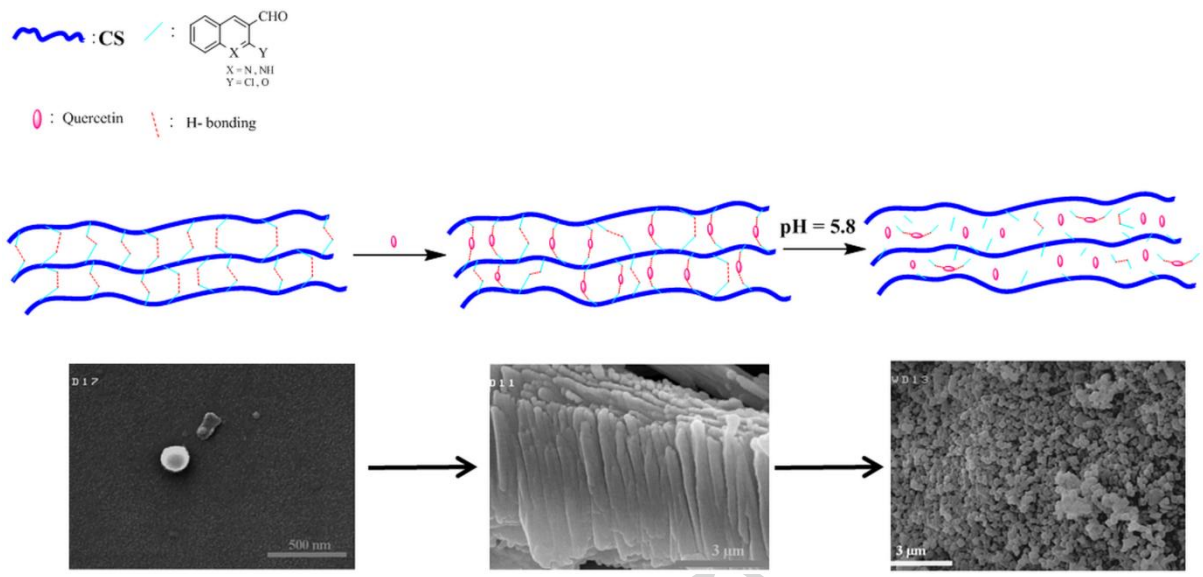

Graphical abstract

Highlights

- Chitosan was crosslinked with quinoline derivatives via O/W nanoemulsion method.
- Chitosan–quinoline nanoparticles were prepared as anticancer drug nanocarriers.
- Quercetin–loaded chitosan–quinoline nanoparticles showed nanorod-like morphology.
- Quercetin–loaded chitosan–quinoline nanoparticles exhibited anticancer properties.